Optical Imaging of Functional Organization in the Monkey Inferotemporal Cortex
Gang Wang, *et al.*
Science **272**, 1665 (1996);
DOI: 10.1126/science.272.5268.1665

directly. It remains to be seen if substrate-induced protein-protein interactions also transmit other nutritional signals. Hexokinase-dependent glucose repression in yeast (*21*) and glucokinase-dependent regulation of glucose homeostasis in mammals (*22*) are possible candidates.

REFERENCES AND NOTES

1. H. Kakidani and M. Ptashne, *Cell* **52**, 161 (1988); J. Ma, E. Przibilla, J. Hu, L. Bogorad, M. Ptashne, *Nature* **334**, 631 (1988); J. A. Fisher, E. Giniger, T. Maniatis, M. Ptashne, *ibid.* **332**, 853 (1988).
2. W. Bajwa, T. E. Torchia, J. E. Hopper, *Mol. Cell. Biol.* **8**, 3439 (1988).
3. P. J. Bhat, D. Oh, J. E. Hopper, *Genetics* **125**, 281 (1990).
4. M. Johnston, *Microbiol. Rev.* **51**, 458 (1987).
5. P. Bhat and J. E. Hopper, *Mol. Cell. Biol.* **12**, 2701 (1992).
6. J. M. Salmeron and S. A. Johnston, *Nucleic Acids Res.* **14**, 7767 (1986); M. I. Riley, J. E. Hopper, S. A. Johnston, R. C. Dickson, *Mol. Cell. Biol.* **7**, 780 (1987); J. M. Salmeron, S. D. Langdon, S. A. Johnston, *ibid.* **9**, 2950 (1989).
7. F. T. Zenke, W. Zachariae, A. Lunkes, K. D. Breunig, *Mol. Cell. Biol.* **13**, 7566 (1993).
8. J. Meyer, A. Walker-Jonah, C. P. Hollenberg, *ibid.* **11**, 5454 (1991).
9. J. Meyer, thesis, Heinrich-Heine-Universität Düsseldorf (1993).
10. Whereas the *gal1* mutant is noninducible, a *gal1 gal80* double mutant has exactly the same constitutive phenotype as a *gal80* mutant (*9*, *23*).
11. The His tag of the sequence Arg-Ser-His_6 was inserted into the linker region of the *K. lactis* Gal80 protein at amino acid position 349. The linker region had been defined by sequence comparison with *S. cerevisiae* Gal80p (ScGal80p) as the only region without sequence and length conservation (*7*). When ^{His}KlGal80p was expressed from the *ADH1* promoter and introduced into a *K. lactis gal80*$^-$ mutant on a multicopy plasmid (pEAG80His), the mutation was fully complemented as assayed by the expression of the Lac9p-controlled β-galactosidase gene.
12. J. Crowe *et al.*, in *Methods in Molecular Biology*, A. J. Harwood, Ed. (Humana, Totowa, NJ, 1990), pp. 371–387.
13. The *Klgal1-m1* mutant was obtained by mutagenesis of a *GAL1*-containing plasmid with hydroxylamine. Regulatory-deficient mutant plasmids were obtained after transformation of a *gal1* strain by screening on X-Gal plates containing 3% glycerol, 2% lactate, and 2% galactose. The wild-type gene resulted in blue colonies because the *K. lactis* β-galactosidase gene was induced, whereas regulatory-deficient *gal1* mutant alleles were white. Among the latter, mutants retaining galactokinase activity were identified by their ability to complement the *gal1-209* allele (reg$^+$ kin$^-$) for growth on galactose [J. Meyer *et al.*, in preparation].
14. β-Galactosidase is encoded by the *LAC4* gene, which is one of the KlGal4p-controlled genes in *K. lactis*. Enzymatic activity is strictly controlled by transcriptional regulation.
15. A *gal80::URA3* disruption was replaced by the *ScGAL80* structural gene fused to the *KlGAL80* promoter.
16. A cell extract from a *gal1 gal80* deletion strain transformed with pEAG80His [compare (*11*)] was loaded on a Ni-NTA-agarose column (3 ml), washed with extraction buffer (50 mM Hepes buffered with NaOH to pH 8, 100 mM NaCl, 10% glycerol) containing 50 mM imidazole, and eluted with a 30-ml linear gradient of 50 to 200 mM imidazole.
17. The GST-KlGal1p fusion was purified from a *gal1* deletion strain transformed with a multicopy plasmid carrying the *Gst-KlGAL1* gene fusion under the *ADH1* promoter. The extract was loaded on a glutathione-agarose column (3 ml) and eluted with extraction buffer containing 10 mM glutathione. ^{His}KlGal80p and GST-KlGal1p fractions were pooled, concentrated by dialysis against 10% polyethylene glycol 20.000 in extraction buffer, and dialyzed against binding buffer (50 mM Hepes buffered with NaOH to pH 8, 100 mM NaCl, 10 mM $MgCl_2$, 7 mM β-mercaptoethanol, 10% glycerol).
18. The *Gst* gene was amplified by polymerase chain reaction from pGEX-3X [D. B. Smith and K. S. Johnson, *Gene* **67**, 31 (1988)] and inserted into an *ADH1-GAL1* construct between the *ADH1* promoter and the *KlGAL1* gene. The gene fusion encodes a protein of 736 amino acids with a molecular mass of ~81 kD with 234 amino acids attached to the NH_2-terminal end of KlGal1p. The galactokinase activity of the fusion protein was comparable with that of the wild-type protein.
19. F. T. Zenke *et al.*, data not shown.
20. K. K. Leuther and S. A. Johnston, *Science* **256**, 1333 (1992).
21. M. Rose, W. Albig, K.-D. Entian, *Eur. J. Biochem.* **199**, 511 (1991).
22. A. Grupe, B. Hultgren, A. Ryan, Y. H. Ma, M. Bauer, T. A. Stewart, *Cell* **83**, 69 (1995).
23. W. Zachariae, thesis, Heinrich-Heine-Universität Düsseldorf (1994).
24. G Ammerer, *Methods Enzymol.* **101**, 192 (1983).
25. M. M. Bianchi *et al.*, *Curr. Genet.* **12**, 185 (1987).
26. Protein extracts from yeast transformants grown in synthetic minimal medium (SM) with 3% glycerol were prepared by glass bead lysis in binding buffer. Extracts were incubated for 1 hour with equilibrated Ni-NTA-agarose at 4°C. Galactose (2%) and 2 mM ATP were added during the binding and washing steps. The resin was washed with binding buffer containing 50 mM imidazole and heated for 10 min at 95°C in SDS sample buffer, followed by fractionation of the proteins by SDS–polyacrylamide gel electrophoresis (SDS-PAGE).
27. F. T. Zenke, thesis, Heinrich-Heine-Universität Düsseldorf (1995).

28. We thank P. Kuger for expert technical assistance and G. Cardinali for supplying the *ADHI–gal1-m1* fusion. Many colleagues, in particular J. Dohmen and R. Kölling, have contributed with helpful critical comments on the manuscript. Supported by Deutsche Forschungsgemeinschaft grant Br921 to K.D.B. and Bundesministerium für Bildung und Forschung–Schwerpunkt Biocatalysis to C.P.H.

7 December 1995; accepted 4 April 1996

Optical Imaging of Functional Organization in the Monkey Inferotemporal Cortex

Gang Wang, Keiji Tanaka,* Manabu Tanifuji

To investigate the functional organization of object recognition, the technique of optical imaging was applied to the primate inferotemporal cortex, which is thought to be essential for object recognition. The features critical for the activation of single cells were first determined in unit recordings with electrodes. In the subsequent optical imaging, presentation of the critical features activated patchy regions around 0.5 millimeters in diameter, covering the site of the electrode penetration at which the critical feature had been determined. Because signals in optical imaging reflect average neuronal activities in the regions, the result directly indicates the regional clustering of cells responding to similar features.

Columnar organization, that is, the clustering of cells with similar response properties in columns running orthogonal to the cortical surface, has been assumed to be a general architecture in the neocortex (*1*). However, the evidence for this is almost entirely limited to the lower stages of sensory pathways. The anterior part of the inferotemporal cortex (the anterior IT) represents the final stage of the visual pathway, which is critical for object recognition. Previous unit recording experiments have shown that cells in the anterior IT selectively respond to moderately complex visual features of objects (*2–4*) and that cells with similar selectivity cluster in columnar regions (*4*, *5*). To confirm the columnar organization in the anterior IT and to further study the spatial organization of the anterior IT columns, we used optical imaging (*6*). Optical imaging is complementary to unit recording for study of spatial organization because in optical imaging the local average of neuronal activities is measured simultaneously over a wide cortical region (*7*).

To find the visual stimuli that were effective for activation of the region of the anterior IT to be subjected to optical imaging and to establish the relation between neuronal activities and optical signals in the anterior IT, we performed unit recordings and optical imaging in two hemispheres (*8*). Unit recordings with electrodes were first conducted in several separate sessions, in which the features of objects critical for the activation of single cells ("critical features") were determined by a reduction method (*9*). In the subsequent optical imaging session, these critical features as well as some simpler stimuli that had been

G. Wang, Laboratory for Neural Information Processing, Frontier Research Program, Institute of Physical and Chemical Research (RIKEN), and Department of Physiology II, Faculty of Medicine, Kagoshima University, 8-35-1 Sakuragaoka, Kagoshima-shi, Kagoshima, 890, Japan.
K. Tanaka, Laboratory for Neural Information Processing, Frontier Research Program, and Information Science Laboratory, RIKEN, 2-1 Hirosawa, Wako-shi, Saitama, 351-01, Japan.
M. Tanifuji, Department of Information Science, Fukui University, and Precursory Research for Embryonic Science and Technology (PRESTO), Research Development Corporation of Japan, 3-9-1 Bunkyo, Fukui, 910, Japan.
*To whom correspondence should be addressed.

ineffective for activating the single cells were used (*10*). The images were obtained without dye, with the use of reflected light at 605-nm wavelength (bandwidth, 10 nm). There is evidence that signals obtained at this wavelength originate mainly in changes in the oxidation level of hemoglobin in capillaries (*11*), although this remains controversial (*12*). In any case, it has been shown that increased neuronal activities result in a decrease in the intensity of reflected light (*13*).

In the present study, the visual stimulation resulted in darkening of the entire image of the exposed anterior IT. This global shift was specific to the visual cortex below the superior temporal sulcus and was absent in the auditory cortex above this sulcus (*14*). In addition to this global darkening, presentation of the critical features specifically evoked the appearance of a few dark spots in the imaged region of the anterior IT. The dark spots are thought to reflect local activation caused by presentation of the visual stimuli for the following three reasons. First, the results are reproducible. The images obtained during the first half of the stimulus repetitions and those obtained during the second half were very similar to each other (*15*). Second, the positions of the dark spots differed from stimulus to stimulus. The significant areas of the dark spots were determined by subtracting from the individual images the mean image ("cocktail reference") averaged over the images obtained for all the different stimuli combined in the series, and then calculating *t* values for individual pixels on the basis of pixel intensities in individual trials. The dark spots evoked by presentation of different critical features covered different regions, although there were a few overlapping regions (Fig. 1). Third, one of the dark spots in each image covered the site of the electrode penetration at which the critical feature was determined (the cross marks in Fig. 1) (*16*).

The stimulus selectivity of the darkening at particular cortical sites is further shown in Fig. 2 for two sites. Presentation of the critical features evoked a dark spot covering the site of penetration at which the critical feature had been determined for a recorded cell in one of the preceding unit recording sessions, whereas the control stimuli proven to be ineffective for the activation of the cell did not cause a darkening at the site (Fig. 2, A and B). Because the critical feature and control stimuli commonly evoked some darkening at some regions distant from the penetration site, a division between two images showed a more isolated dark spot. The regions did not become dark at all or became very slightly dark upon presentation of 11 other critical features determined for cells recorded in different penetrations or presentation of other control stimuli (Fig. 2C) (*17*).

The dark spots were circular or elliptic, and the width at $1/e$ (~0.37) drop from the peak ranged from 0.33 to 0.67 mm with a mean and SD of 0.49 and 0.11 mm, respectively. Because the metabolic change was expected to be observable only upon activation of a large population of cells in the region, these results suggest local clustering of cells responding to the same feature. The diameter of the spots roughly corresponded to the width of clusters of cells with similar selectivities that was determined in our previous unit recording experiment (0.4 ± 0.2 mm) (*4*). The number of dark spots (with *t* values giving $P < 0.01$, in reference to the cocktail reference) evoked by each critical feature within the imaged region of the anterior IT (6.1 × 3.3 mm) varied from 2 to 10. However, this does not indicate that all of these spots required the presence of all the features included in the stimulus to be evoked. Some of the spots may have been evoked by simpler features. Actually, in the two cases shown in Fig. 2, a division of the image by the image evoked by a simpler stimulus that is a component of the critical feature reduced the number of dark spots to one or two.

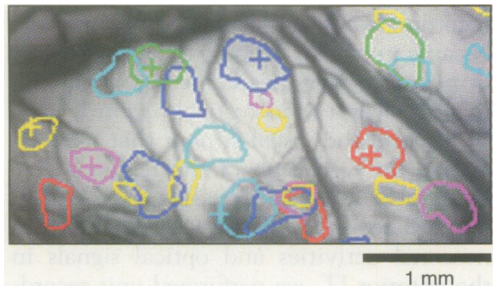

Fig. 1. Dependence of image pattern on visual stimuli. The contours of dark spots evoked by six different critical features (indicated by red, yellow, green, turquoise, indigo, and magenta) are superimposed on the blood vessel image. The contours were defined by the distribution extents of pixels, with *t* values giving $P < 0.05$. The sites of the electrode penetrations at which the critical features were determined are indicated by cross marks of corresponding color.

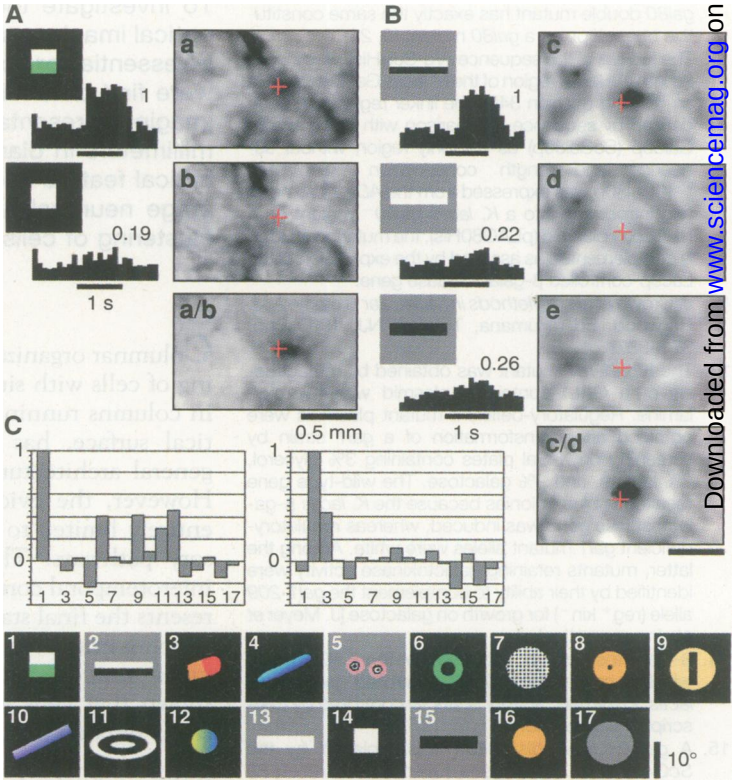

Fig. 2. The correlation between neuronal activities and optical changes, illustrated for two cortical sites. (**A**) Poststimulus time histograms of responses evoked in the cell for which the critical feature was determined in the unit recording session (averaged over 10 trials, left) and the images evoked by the stimuli in the optical imaging session (right) are aligned. The numbers above the histograms represent the relative magnitude of the cell responses, and the underscores indicate the 1-s period of stimulus presentation. The red cross marks in the images at right indicate the site of the penetration in which the cell was recorded. The image at the bottom (a/b) was obtained by dividing the image obtained with the critical feature (a) by that obtained with its control stimulus (b). (**B**) The same as (A) but for another cell and site. Shown are the image obtained with the critical feature (c), the images obtained with its control stimuli (d and e), and the division between c and d. (**C**) The level of darkening was calculated for the two regions [top left panel for the region shown in (A); top right panel for the region shown in (B)] in the images obtained with the critical feature determined at the site, with 11 other critical features determined for cells recorded in different penetrations, and with five simpler control stimuli (the 13th to 17th stimuli). The numbers along the *x* axis represent the stimulus number. To calculate the level of darkening (*y* axis), a spot was set around the penetration site, and the image intensity averaged over a ring-shaped region circumscribing the spot was subtracted from the image intensity averaged over the region within the spot. The values were normalized by the maximal darkness evoked by the critical feature at the site. The numbered stimuli are illustrated at the bottom.

In one electrode penetration, five cells were recorded and all of them selectively responded to faces. Three of them responded maximally to the front face, whereas the other two responded maximally to the profile (lateral view of the face). Although we failed to identify the exact site of the penetration in this case, five different views of the same doll face evoked overlapping dark spots around the site of the penetration (Fig. 3A). The contours of the spots, defined either by 1/*e* drop from the peak or by the distribution extent of pixels with *t* values giving $P < 0.01$ or $P < 0.05$, moved systematically in one direction as the face was turned from the left profile to the right profile through the 45° left, front, and 45° right faces. The length of the overall region along the direction of movement was 0.8 mm for the 1/*e* contours.

Similar results, that is, the selective activation by faces and systematic shift of the activation spot with the viewing angle, were obtained in two other hemispheres (Fig. 3, B and C) (*18*). In the case shown in Fig. 3C, nearly the same set of activation was repeated by the rotation of the doll face (left) and that of a living human face (right). The slight possibility that displacements of some part of the face that accompanied the rotation caused the shift of activation was excluded because when the front face was shifted to three different horizontal positions, it activated nearly the same center regions (*19*). The activation of these regions was specific to faces (*20*). Presentation of the faces evoked a few other dark spots at different locations, but the positions of these spots did not move systematically with the rotation of the face.

The latter results (shown in Fig. 3) suggest that there are continuous maps of related features in the anterior IT. Whether the continuous mapping of related features is specific to different views of faces or is generally used in the anterior IT remains to be determined, as does whether or not a single map continues for a large region of the anterior IT. Considering the high dimensionality of the feature space that the anterior IT has to represent, its map on the two-dimensional cortical surface should be divided into multiple compartments (*21*). The borders between the cortical regions representing related but different features were not discrete; there was overlapping of regions. Each of the cells in overlapping regions may have responded to the different stimuli without clear discrimination, or different groups of cells responding to the different stimuli may have been intermingled in the region. An alternative possibility that the apparent overlaps were caused by expansion of the metabolic changes beyond neuronal activities is not likely because cells responding to the different stimuli were recorded in the same vertical penetration, as described above.

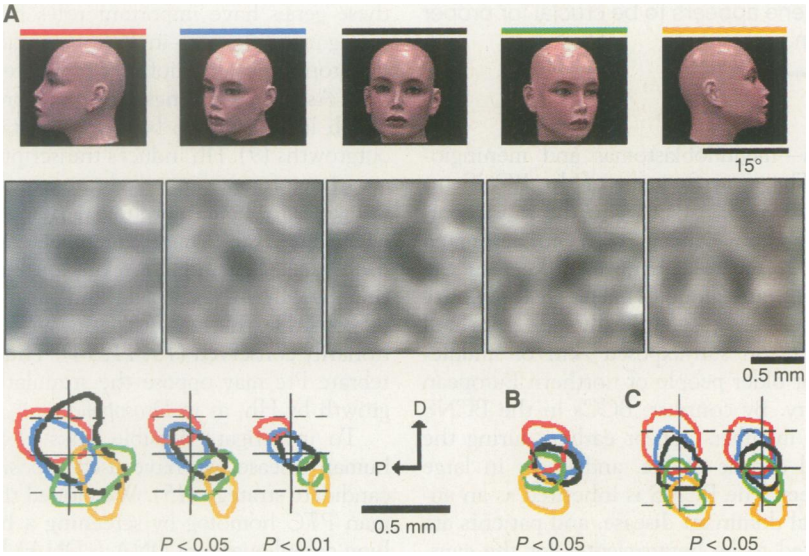

Fig. 3. Systematic movement of the activation spot with rotation of the face. (**A**) Images of the same cortical area (middle panels) obtained for five different views of the same doll face (top panels). The cocktail reference obtained by averaging of the five images has been subtracted. The contours of the dark spots are magnified and superimposed at the bottom. The colors of the contours indicate the view that evoked the dark spot (red, left profile; blue, left 45°; black, front; green, right 45°; and yellow, right profile). (**B**) and (**C**) Similar results obtained in two other hemispheres. The same set of viewing angles was used as in (A). The face of a living human was used in (B), and both the doll face (left-hand pattern) and the human face (right-hand pattern) were used in (C). The positional relations between contours in different drawings in (A) and (C) can be examined by alignment of the vertical and horizontal straight lines. The arrows indicate the dorsal (D) and posterior (P) directions in the images.

Thus, by using optical imaging in combination with unit recordings, we have confirmed the regional clustering of cells responding to similar features in the anterior IT. We also obtained evidence suggesting that there is continuous mapping of related features over a region around 1 mm in size in the anterior IT.

REFERENCES AND NOTES

1. V. B. Mountcastle, *The Mindful Brain* (MIT Press, Cambridge, MA, 1978), pp. 7–50.
2. C. G. Gross, C. E. Rocha-Miranda, D. B. Bender, *J. Neurophysiol.* **35**, 96 (1972); R. Desimone, T. D. Albright, C. G. Gross, C. Bruce, *J. Neurosci.* **4**, 2051 (1984).
3. K. Tanaka, H. Saito, Y. Fukada, M. Moriya, *J. Neurophysiol.* **66**, 170 (1991); E. Kobatake, K. Tanaka, *ibid.* **71**, 856 (1994); M. Ito, I. Fujita, H. Tamura, K. Tanaka, *Cereb. Cortex* **5**, 499 (1994); M. Ito, H. Tamura, I. Fujita, K. Tanaka, *J. Neurophysiol.* **73**, 218 (1995).
4. I. Fujita, K. Tanaka, M. Ito, K. Cheng, *Nature* **360**, 343 (1992).
5. P. M. Gochin, E. K. Miller, C. G. Gross, G. L. Gerstein, *Exp. Brain Res.* **84**, 505 (1991).
6. A. Grinvald, R. D. Frostig, E. Lieke, R. Hildesheim, *Physiol. Rev.* **68**, 1285 (1988).
7. D. Y. Ts'o, R. D. Frostig, E. E. Lieke, A. Grinvald, *Science* **249**, 417 (1990); T. Bonhoeffer and A. Grinvald, *Nature* **353**, 429 (1991); G. G. Blasdel, *J. Neurosci.* **12**, 3115 (1992); *ibid.*, p. 3139; D. Malonek, R. B. H. Tootell, A. Grinvald, *Proc. R. Soc. London B* **258**, 109 (1994); D.-S. Kim and T. Bonhoeffer, *Nature* **370**, 370 (1994); A. Das and C. D. Gilbert, *ibid.* **375**, 780 (1995).
8. The present data were obtained from four hemispheres of three adult macaque monkeys (*Macaca fuscata*). For two of the four hemispheres, unit recordings with electrodes were conducted in several separate sessions over 2 to 3 months, and a separate optical imaging session was conducted thereafter. Only optical imaging was conducted in the other two hemispheres. Monkeys were anesthetized with N_2O (70%) and isoflurane (up to 2%) and immobilized with pancuronium bromide in electrode recording and optical imaging sessions, and all the procedures were performed under aseptic conditions. Monkeys were regularly monitored by a veterinarian and cared for in accordance with the "Guiding Principles for the Care and Use of Animals in the Field of Physiological Science" of the Japanese Physiological Society.
9. After activity from a single cell was isolated, many three-dimensional objects were first presented to determine effective stimuli, and then the image of the most effective stimulus was simplified successively to determine the critical feature. For details of this reduction process, see (*3, 4*).
10. Before the optical imaging, a chamber 18 mm in diameter was attached to the skull, the skull and the dura covering the imaged region were removed, and the chamber was filled with silicone oil to minimize movement of the brain. We measured the intrinsic signals by illuminating the cortex with two fiber-optic lights and obtaining images with an Imager 2001 (Optical Imaging) equipped with a charge-coupled-device camera. The visual stimuli were presented on a 20-inch television monitor 40 or 28 times each for 4 s at 8- or 14-s intervals. The stimulus image was presented suddenly on the prestimulus homogeneously gray screen and then moved in a circular path (with a radius of 0.4° at a rate of 1 cycle/s) for 4 s. The background of the stimulus image was the same as the prestimulus homogeneous gray. Five to 28 different stimuli, together with a few nonstimulus conditions, were combined and presented in circular order, and image processing (division and subtraction) was performed only between the images obtained within the combined conditions. The image frames obtained during individual responses were averaged over the period from 0.5 s after the stimu-

lus onset to the stimulus offset. This response image was divided by the image obtained during a blank screen period ("blank reference") to compensate for the difference in the background level of reflected light. From the image, then, was subtracted the image obtained by division between the image obtained in the 1-s period just before the stimulus onset and the corresponding image of the blank reference, in order to compensate for slow changes in signals over several minutes. No spatial filtering except smoothing (high-cut filtering) was performed.
11. R. D. Frostig, E. E. Lieke, D. Y. Ts'o, A. Grinvald, *Proc. Natl. Acad. Sci. U.S.A.* **87**, 6082 (1990).
12. B. A. MacVicar and D. Hochman, *J. Neurosci.* **11**, 1458 (1991).
13. A. Grinvald, E. Lieke, R. D. Frostig, C. D. Gilbert, T. N. Wiesel, *Nature* **324**, 361 (1986); A. Grinvald, R. D. Frostig, R. M. Siegel, E. Bartfeld, *Proc. Natl. Acad. Sci. U.S.A.* **88**, 11559 (1991); M. M. Haglund, G. A. Ojemann, D. W. Hochman, *Nature* **358**, 668 (1992); P. M. Gochin, P. Bedenbaugh, J. J. Gelfand, C. G. Gross, G. L. Gerstein, *Proc. Natl. Acad. Sci. U.S.A.* **89**, 8381 (1992); S. A. Masino, M. C. Kwon, Y. Dory, R. D. Frostig, *ibid.* **90**, 9998 (1993).
14. The t values calculated on a trial-by-trial basis for the deviation from 1 of the mean for the pixels below the sulcus gave $P < 0.01$ for all of the 19 stimuli examined, whereas those calculated for pixels above the sulcus gave $P > 0.1$ for 17 stimuli and $P > 0.05$ for the remaining 2 stimuli.
15. The coefficient of cross-correlation calculated on a pixel-by-pixel basis for the anterior IT region was 0.65 ± 0.04 ($n = 19$). These values had no overlap with the correlation coefficients calculated between images obtained with different critical features (0.30 ± 0.08, $n = 91$).
16. The sites of electrode penetration were pinpointed with ink directly on the cortical surface and were successfully identified at the time of optical imaging for 13 penetrations. In 10 out of the 13 cases, the penetration site was enclosed by the contour of the dark spot defined by a drop from the peak by $1/e$ of the difference between the peak and the average of the surrounding regions. In another case, the penetration site was at a $2/e$ drop from the peak, and in the other two cases the penetration site was distant from the dark spots.
17. Calculation of t values for individual pixels, in reference to the cocktail references, showed that the darkening evoked by the critical feature determined at the site was statistically significant ($P < 0.01$) but that the other stimuli evoked no significant darkening around the region ($P > 0.10$).
18. Only optical imaging was conducted in these two hemispheres. The main purpose of these experiments was to repeat the systematic movement of the activation spot with the rotation of the face. Ten or 14 nonface stimuli were also presented in order to examine the selectivity of activation.
19. G. Wang, K. Tanaka, M. Tanifuji, data not shown.
20. None of the nonface stimuli [10 stimuli in the cases shown in Fig. 3, A and C, and 14 stimuli in the case shown in Fig. 3B] evoked a statistically significant darkening around the regions ($P > 0.10$).
21. D. H. Ballard, *Behav. Brain Sci.* **9**, 67 (1986).
22. Supported by the Frontier Research Program, RIKEN.

22 December 1995; accepted 16 April 1996

Human Homolog of *patched*, a Candidate Gene for the Basal Cell Nevus Syndrome

Ronald L. Johnson, Alana L. Rothman, Jingwu Xie, Lisa V. Goodrich, John W. Bare, Jeannette M. Bonifas, Anthony G. Quinn,* Richard M. Myers, David R. Cox, Ervin H. Epstein Jr.,† Matthew P. Scott†

The basal cell nevus syndrome (BCNS) is characterized by developmental abnormalities and by the postnatal occurrence of cancers, especially basal cell carcinomas (BCCs), the most common human cancer. Heritable mutations in BCNS patients and a somatic mutation in a sporadic BCC were identified in a human homolog of the *Drosophila patched (ptc)* gene. The *ptc* gene encodes a transmembrane protein that in *Drosophila* acts in opposition to the Hedgehog signaling protein, controlling cell fates, patterning, and growth in numerous tissues. The human *PTC* gene appears to be crucial for proper embryonic development and for tumor suppression.

Patients with the BCNS (also called Gorlin syndrome; Mendelian Inheritance in Man, No. 109400) have diverse developmental abnormalities, often including rib and craniofacial alterations and, less often, polydactyly, syndactyly, and spina bifida (*1*). In addition, these patients suffer from a multitude of tumor types. These include fibromas of the ovaries and heart; cysts of the skin, jaws, and mesentery; and the more devastating cancers of the central nervous system—medulloblastomas and meningiomas. The most frequent of the BCNS tumors are BCCs. BCCs are the most common human cancer, with an estimated 750,000 cases occurring each year in the United States alone (*2*). The great majority of BCCs arise sporadically and in small numbers on sun-exposed skin of middle-aged or older people of northern European ancestry. By contrast, BCCs in the BCNS family members appear earlier, during the second decade of life, and occur in large numbers. The BCNS is inherited as an autosomal dominant disease, and patients are expected to be heterozygotes for the causative mutation.

The *ptc* gene, identified initially as a *Drosophila* segment polarity gene (*3*), encodes a transmembrane protein that is produced in precise spatial patterns in developing flies (*4*). The *ptc* gene controls development by repressing transcription, in specific cells, of genes encoding members of the transforming growth factor-β (TGF-β) and Wnt families of signaling proteins. These genes are induced by a signal from the Hedgehog (Hh) protein, which counters repression by Patched (Ptc). Ectopic expression of Hh in *Drosophila* imaginal discs, which are precursors of adult body structures, stimulates growth and causes appendage duplication (*5*, *6*), whereas ectopic expression of Ptc inhibits growth, causing development of smaller than normal wings (*7*).

Vertebrate homologs of *hh* and *ptc* have been identified in mice, chickens, and zebrafish (*8*–*11*). Human *HH* genes have also been described (*12*). The patterns of *ptc* and *hh* expression in vertebrates suggest that these genes have important roles in organizing many tissues—including neural tube, skeleton, limbs, craniofacial structures, and skin. As in insect wings, ectopic expression of Hh in chick limb buds causes dramatic outgrowths (*9*). Hh induces transcription of a variety of genes in vertebrates, including the genes for bone morphogenetic proteins, which are TGF-β family members, and *ptc* itself (*13*). The induction of *ptc* transcription by Hh in *Drosophila* and vertebrates suggests that the Hh–Ptc pathway is evolutionarily conserved (*10*, *11*, *14*). Thus, vertebrate Ptc may oppose the stimulation of growth by Hh, as in *Drosophila*.

To investigate possible links of *ptc* to human disease, we have used a positional candidate strategy (*15*). We cloned the human *PTC* homolog by screening a human lung complementary DNA (cDNA) library with several mouse *ptc* cDNA probes (*16*). Several partial human *PTC* cDNAs were identified and sequenced to obtain the entire coding sequence. Thus far we have found only one human gene, although we have not performed an exhaustive search for related genes. The assembled 5.1 kilobases (kb) of contiguous sequence contains a 4.5-kb open reading frame (ORF) encod-

R. L. Johnson, L. V. Goodrich, M. P. Scott, Departments of Developmental Biology and Genetics, Howard Hughes Medical Institute, Stanford University School of Medicine, Stanford, CA 94305–5427, USA.
A. L. Rothman, J. Xie, J. W. Bare, J. M. Bonifas, A. G. Quinn, E. H. Epstein Jr., Department of Dermatology, San Francisco General Hospital, University of California, San Francisco, CA 94110, USA.
R. M. Myers and D. R. Cox, Department of Genetics, Stanford University School of Medicine, Stanford, CA 94305, USA.

*Present address: Department of Dermatology, St. Bartholomew's and the Royal Hospital School of Medicine, London, UK.
†To whom correspondence should be addressed.